Table of Contents

CHAPTER 5.

CHAPTER 5.

Atmospheric Boundary-Layer Modelling

Turbulent shear flows arise in many areas of fluid mechanics. In most instances they are limited in physical extent and in numbers of people affected. However, one deep turbulent shear flow - the atmospheric boundary layer - impinges upon us all and it seems worthwhile, if not imperative, to make an effort to understand and model it.

Dynamically, however, the atmospheric boundary layer (ABL) is far more complex than most "engineering" flows for it involves:

- temporal and spatial variation;
- buoyancy forces;
- Coriolis forces.

For this reason we should not expect turbulence models designed and calibrated in engineering laboratories to work well without modification in atmospheric flows. Nor are alternative models easy to validate: the depth of the ABL, typically between 100 and 2000m, makes it less amenable to experimental measurement than boundary-layer flows of more limited extent.

Coriolis forces arise from fluid motions observed on a rotating reference frame called the earth. They lead to the large circulatory systems around pressure "highs" and "lows" on our weather maps. Locally, they lead to a turning of the wind with height.

The density differences responsible for buoyancy forces arise from differential heating and cooling. On a hot day the ground and the air next to it are heated by solar radiation, driving convection and generating a deep, well-mixed, turbulent layer. In the absence of an external source of heat at night the ground cools by radiation and a stably stratified layer develops. Buoyancy forces then inhibit vertical motions - both the mean flow around terrain undulations and the turbulent fluctuations responsible for the cross-stream transport of heat and momentum. Since these same fluctuations are responsible for diffusing pollutants it becomes important to parameterise the effects of buoyancy in turbulence models.

Perhaps the hardest aspects of the ABL to model are temporal and spatial inhomogeneities. Time-dependence of the radiation balance is forced by the diurnal and seasonal variational of incoming solar radiation (which is predictable) and is complicated by latent heat transport and the evolution of clouds (which is not - much). Spatial inhomogeneities may arise from variations in surface properties (for example, elevation, roughness, albedo and water content) and from the passage of large-scale features such as weather fronts. However, there is evidence that, under uniform surface conditions and provided the rate of surface cooling is not such as to eradicate turbulence, quasi-equilibrium states may be attained by the ABL (Mason and Derbyshire, 1990) and this will be implicit in what follows.

5.1 Atmospheric Boundary-Layer Equations

Throughout this Chapter we shall consider an idealised, horizontally homogeneous, atmospheric boundary layer (ABL) over a flat plane, wherein the mean velocity $\vec{U} \equiv (U, V, \mathbf{0})$ and potential temperature Θ are functions of the vertical coordinate z alone. Since there is no mean vertical motion the flow is in hydrostatic balance:

$$\frac{\partial \boldsymbol{P}}{\partial z} = -\rho \boldsymbol{g} \tag{5.1}$$

and as density is a function of z only it follows that $\partial^2 P/\partial x \partial z = \partial^2 P/\partial y/\partial z = 0$, and hence that the horizontal pressure gradients $\partial P/\partial x$, $\partial P/\partial y$ are independent of height; (ie, the boundary layer is *barotropic*).

5.1.1 Mean-Velocity Equations

The Navier-Stokes equations give for the horizontal components of momentum:

$$\frac{DU}{Dt} = -\frac{1}{\rho}\frac{\partial P}{\partial x} + fV + \frac{\partial \tau_{xz}}{\partial z}$$
$$\frac{DV}{Dt} = -\frac{1}{\rho}\frac{\partial P}{\partial y} - fU + \frac{\partial \tau_{yz}}{\partial z} \qquad (5.2)$$

where $(\tau_{xz},\tau_{yz})=(-\overline{u'w'}, -\overline{v'w'})$ are the non-zero components of the (kinematic) shear stress and $f=2\Omega\sin\lambda$ is the Coriolis parameter. (Ω is the angular rotation rate of the earth and λ the latitude. At mid-latitudes, $f\approx 10^{-4}s^{-1}$). For large z the mean-velocity components are assumed to approach constant values (U_g,V_g) and the horizontal shear stresses (τ_{xz},τ_{yz}) to vanish. Under horizontally homogeneous, steady-state conditions the advection terms disappear and the constant pressure gradients can be written in terms of the *geostrophic* wind velocities prevailing at the top of the boundary layer:

$$U_g = -\frac{1}{\rho f}\frac{\partial P}{\partial y}, \qquad V_g = \frac{1}{\rho f}\frac{\partial P}{\partial x} \qquad (5.3)$$

The boundary-layer equations then reduce to

$$\frac{\partial \tau_{xz}}{\partial z} = -f(V-V_g)$$
$$\frac{\partial \tau_{yz}}{\partial z} = f(U-U_g) \qquad (5.4)$$

or, more conveniently, in complex variable notation:

$$\frac{\partial \tau}{\partial z} = if(W-W_g) \qquad (5.5)$$

where $\tau=\tau_{xz}+i\tau_{yz}$, $W=U+iV$.

Vertical profiles of U and V require a closure model for the shear stress which will be discussed below. However, two points about the presence of Coriolis forces are worth making here.

The first is that most numerical models of the ABL consider only a uni-directional approach

flow. However, without Coriolis forces a horizontally homogeneous boundary layer is not possible - the boundary layer must grow. (Mathematically, $\partial\tau/\partial z$=*constant* implies that τ is either constant or varies linearly with height - indefinitely). At the top of the boundary layer where the stress divergence vanishes the Coriolis force must balance the applied pressure gradient. This apparently trivial point nevertheless *precludes the modelling of pressure-driven boundary layers as uni-directional flow with periodic boundary conditions*.

The second point concerns a little numerical difficulty in the iterative solution of the boundary-layer equations. If we assume for the moment that the shear stress is given by some *constant* eddy viscosity ν_t then

$$\tau = \nu_t \frac{\partial W}{\partial z} \tag{5.6}$$

and equation (5.5) becomes

$$\frac{\partial^2 W}{\partial z^2} = \frac{if}{\nu_t}(W - W_g) \tag{5.7}$$

with solutions

$$W - W_g = -W_g e^{\pm (f/2\nu_t)^{1/2}(1+i)z} \tag{5.8}$$

(We have adopted the somewhat partisan assumption that f is positive; ie, we are in the northern hemisphere. Those from down-under may replace f by $|f|$ and $1+i$ by $1-i$). The negative sign should be taken in the exponent to give the appropriate asymptotic limit $W \to W_g$ as $z \to \infty$ (and the classical 45° turning of the wind over the depth of the boundary layer - Ekman, 1905). However, without a little caution it is quite possible for an iterative numerical solution to pick up the growing exponent, leading to rapid divergence. To illustrate this, consider the centred spatial difference form of (5.7) which can be written as

$$W_k - \tfrac{1}{2}(W_{k+1} + W_{k-1}) = -i\xi(W_k - W_g) \ , \qquad \xi = \frac{f\Delta^2}{2\nu_t} \tag{5.9}$$

on a regular mesh of spacing Δ. Now this system is tri-diagonal and hence soluble in its own right for the complex velocity $\{W_k\}$ given appropriate boundary conditions. It is satisfied, for

example, by $W_k \equiv W_g$. A difficulty arises, however, in the use of the finite-volume code described in Chapter 3 where the system (5.9) is solved iteratively and componentwise by alternating between U and V equations and using the most recent values for the source terms on the RHS. A small error V_{k0} at point k_0 first produces a perturbation in U of order ξV_{k0} and then a perturbation in V of order $-\xi^2 V_{k0}$. (This is not the precise solution, which depends on the nature and location of the boundaries. It does, however, correctly describe the magnitude of the perturbation.) Sequential iteration, therefore, produces an exponentially growing instability if $\xi>1$, which can only be prevented by placing an unsatisfactory restriction on the mesh scale Δ. Relaxation helps a little, the condition for stability becoming $r\xi<1$, but this has the disadvantage of slowing down convergence. To overcome this problem we have employed a form of local relaxation which has little effect in the fine-mesh regions where there are high gradients, but prevents numerical instabilities growing in the coarse-mesh regions at the top of the boundary layer where U and V depart little from their free-stream values U_g and V_g. In the complex equation (5.9) this amounts to replacing the explicit value W_k^* from the previous iteration on the RHS by the implicit $W_k^* - i\xi(W_k - W_k^*)$. The iterative version of equation (5.9) can then be written

$$(1+\xi^2)W_k - \tfrac{1}{2}(W_{k+1}+W_{k-1}) = -i\xi(W_k^* - W_g) + \xi^2 W_k^* \qquad (5.10)$$

and it can be shown that perturbations from the geostrophic solution ($W_k \equiv W_g$) are reduced by a factor of order $\left(\frac{\xi^2}{1+\xi^2}\right)^2 < 1$, stabilising the iterative solution.

5.1.2 Mean Temperature Profile and the Effect of Buoyancy Forces

Due to the diurnal cycle of solar radiation the ABL is seldom in a state of thermal equilibrium and temperature variations occur which cause density variations and hence a change in gravitational forces. Where there is no mean vertical motion the gravitational force is balanced by a pressure gradient according to the hydrostatic relation (5.1). Departures from equilibrium - in particular, turbulent fluctuations - lead to a net buoyancy force per unit mass

$$-\frac{(\rho-\rho_a)}{\rho_a}g = \alpha g(\theta-\theta_a) \tag{5.11}$$

where subscript *a* denotes ambient conditions. $\alpha = -\frac{1}{\rho}\left(\frac{\partial\rho}{\partial T}\right)_p$ is the coefficient of expansion, equal to $1/T$ for perfect gases.

Buoyancy forces affect the mean-velocity profiles in two ways: directly, as a source term in the momentum equation; and indirectly, by their effect on the turbulent shear stress. In stably stratified flows the restoring forces brought about by the former can give rise to gravity (or *internal*) wave motions. In this Chapter, however, we shall assume a horizontally homogeneous boundary layer with no mean vertical motion. Buoyancy effects, therefore, will be confined to turbulence. In the turbulent kinetic energy equation they appear as a source term (negative in stable conditions):

$$G = -g\frac{\overline{\rho' w'}}{\rho_0} = \alpha g\overline{\theta' w'} \tag{5.12}$$

The vertical heat flux is $\rho c_p \overline{\theta' w'}$.

Now, we have postulated the existence of a steady-state stable boundary layer. But if there is a net loss of heat to the ground with no compensating heat flux at the top of the layer then the boundary layer as a whole must cool. We must, therefore, relax our definition somewhat. Following Nieuwstadt (1984, 1985) we define a *steady-state* ABL to be one in which the *turbulent fluxes* (and thence, by assumption, the mean vertical gradients) are independent of time. Both theoretical investigation and numerical studies (Derbyshire, 1990; Mason and Derbyshire, 1990) indicate that, provided the surface cooling is not too extreme, the ABL may indeed approach such a quasi-equilibrium state, with a relaxation time of $O(f^{-1})$. Derbyshire demonstrates theoretically that for given synoptic parameters (surface buoyancy flux and geostrophic wind speed) the (thermal) boundary-layer depth *h* cannot grow indefinitely. Essentially this is because to maintain turbulence the integrated working of buoyancy forces over the depth of the layer must be less than the overall production by shear stresses, which can be bounded above by a factor involving the geostrophic wind speed and surface drag coefficient alone.

Consider the consequences of this quasi-steady-state assumption for the (potential) temperature equation:

$$\frac{\partial \Theta}{\partial t} = -\frac{\partial}{\partial z}(\overline{\theta' w'}) \tag{5.13}$$

(We have ignored the small molecular component of the heat flux.) Taking derivatives with respect to t or z and assuming $\overline{\theta' w'}$ and $\partial\Theta/\partial z$ are independent of time we deduce that:

(i) the boundary layer as a whole cools at a constant rate: $\partial\Theta/\partial t = constant$;

(ii) the heat flux varies linearly with height; ie,

$$\overline{\theta' w'} = \overline{\theta' w'}_0 (1 - z/h) \tag{5.14}$$

Meteorological evidence from Cabauw in the Netherlands (Nieuwstadt, 1984) lends some support for this.

Numerically, global cooling may be incorporated within a steady-state one-dimensional boundary-layer model by solving for the *temperature difference* between each field point and a reference point; (for example, the surface). The constant cooling rate then appears as a source term on the RHS of the potential temperature equation:

$$\frac{D}{Dt}(\Theta - \Theta_r) = -\frac{\partial \Theta_r}{\partial t} - \frac{\partial}{\partial z}(\overline{\theta' w'}) \tag{5.15}$$

where, if h and $\overline{\theta' w'}_0$ are supplied, $\partial\Theta_r/\partial t$ is given by

$$\frac{\partial \Theta_r}{\partial t} = \begin{cases} \dfrac{\overline{\theta' w'}_0}{h} & z<h \\ 0 & z>h \end{cases} \tag{5.16}$$

Since the LHS of (5.15) vanishes this gives the desired linear variation of heat flux with height. However, the model cannot generate the inversion (temperature jump) which must, in practice, develop at $z=h$ to accommodate the net loss of heat from the boundary layer.

5.2 Surface-Layer Similarity Theory

The balance of Coriolis forces and stress divergence in equation (5.2) gives an estimate of the relative change in the shear stress over height Δz:

$$\frac{\Delta\tau}{\tau_0} \sim \frac{fU_g}{u_*^2}\Delta z \tag{5.17}$$

Hence the shear stress may be regarded as essentially constant (u_*^2) over height $\Delta z \ll c_g^2 U_g/f$, where $c_g=u_*/U_g$ is a surface drag coefficient. Typical values for a neutrally stable boundary layer at mid-latitudes are c_g=0.05, U_g=10 m s^{-1}, f=10^{-4}s^{-1}, giving a height scale 250m.

A remarkably successful similarity theory has been built up for this (uni-directional) constant-stress surface layer. For neutrally stable flows well above any rough surface undulations the only available velocity and length scales are the friction velocity u_* and height z, so that

$$\frac{z}{u_*}\frac{dU}{dz} = constant = \frac{1}{\kappa} \tag{5.18}$$

where κ is a universal constant (Von Karman's constant) with a value of approximately 0.4. This integrates immediately to give the well-known logarithmic wind profile:

$$U = \frac{u_*}{\kappa z}\ln(z/z_0) \tag{5.19}$$

with *roughness length* z_0 depending on the nature of the surface.

For boundary layers subject to surface heating or cooling an additional dimensional parameter is available: the surface heat flux $Q_H=\rho c_p\overline{\theta' w'}$ or, derived from it, the buoyancy flux (for ideal gases):

$$G = \alpha g\overline{\theta' w'} = \frac{gQ_H}{\rho c_p T} \tag{5.20}$$

Again, this turbulent flux may be regarded as constant over a (somewhat shallower) surface layer. Comparing production or removal of turbulent kinetic energy by buoyancy forces (G)

with production by shear ($P \sim u_*^3/\kappa z$) we find that there is a height scale L_{MO} where the two terms are of comparable magnitude. L_{MO}, the *Monin-Obukhov length*, is given by

$$L_{MO} = \frac{u_*^3}{\kappa(-G)} \tag{5.21}$$

and, with this sign convention, L_{MO} is positive or negative in stable or unstable conditions respectively.

The presence of a second length scale means that the dimensionless combination $\frac{z}{u_*}\frac{dU}{dz}$ must be a function of z/L_{MO}. We write

$$\frac{z}{u_*}\frac{dU}{dz} = \frac{1}{\kappa}\phi_M(z/L_{MO}) \tag{5.22}$$

with $\phi_M(0)=1$ to conform to the neutral limit.

Arya (1982) and Pasquill and Smith (1983) list empirical and theoretical expressions for the similarity function ϕ_M in stable and unstable boundary layers. We shall confine attention to the stable case for which a well-established form is

$$\phi_M = 1+\beta z/L_{MO}\ , \qquad \beta \approx 5 \tag{5.23}$$

With (5.23) equation (5.22) integrates to give a log-linear profile

$$U = \frac{u_*}{\kappa}[\ln(z/z_0)+\beta z/L_{MO}] \tag{5.24}$$

which is well-attested by surface-layer data.

Similarity theory is not restricted to the mean velocity but may also be used to deduce profiles for scalar variables - passive or otherwise. In this case a scale magnitude may be determined from the vertical flux via

$$F_\theta \equiv \overline{\theta' w'} = -\theta_* u_* \tag{5.25}$$

Then

$$\frac{z}{\theta_*}\frac{d\Theta}{dz} = \frac{1}{\kappa}\phi_H(z/L_{MO}) \tag{5.26}$$

For potential temperature we have typically

$$\phi_H = \sigma_\phi + \beta' z/L_{MO} \tag{5.27}$$

where $\sigma_\phi \approx 0.7$, $\beta' \approx 5$. θ_* and L_{MO} are related by

$$\theta_* = \frac{u_*^2}{\kappa\alpha g L_{MO}} \tag{5.28}$$

Before moving on to consider the boundary layer as a whole it is appropriate to make some additional remarks which will influence the matching of surface and Ekman layers.

(i) Similarity relations (5.22) and (5.26) for the mean velocity and potential temperature profiles are equivalent to gradient-transfer relations with height-dependent eddy diffusivities

$$\begin{aligned} K_M &= \kappa u_* z/\phi_M \\ K_H &= \kappa u_* z/\phi_H \end{aligned} \tag{5.29}$$

(ii) The potential temperature profile deduced from (5.26) and (5.27) is often observed to be a good approximation far above its theoretical limit $z \sim L_{MO}$. In the limit as $z/L_{MO} \to \infty$ the profile tends to one of uniform gradient with buoyancy frequency N given by

$$N \equiv \left(\alpha g \frac{d\Theta}{dz}\right)^{1/2} \to \sqrt{\beta'}\frac{u_*}{\kappa L_{MO}} \tag{5.30}$$

In addition the gradient Richardson number Ri and flux Richardson number R_f defined by

$$Ri = \frac{\alpha g \dfrac{d\Theta}{dz}}{\left|\dfrac{d\vec{U}}{dz}\right|^2}, \qquad R_f = \frac{\alpha g(-\overline{\theta' w'})}{\vec{\tau}.\dfrac{d\vec{U}}{dz}} \tag{5.31}$$

tend to constant values β'/β^2 and $1/\beta$ respectively, or, roughly, 0.2-0.25 with commonly accepted values.

5.3 Local Scaling: Nieuwstadt's Model

Surface-layer theory is applicable only for $z \leq L_{MO}$. In moderate to high stability, where $L_{MO}/h \ll 1$, it provides a means of matching to the surface boundary conditions but says little about mean flow profiles in the boundary layer as a whole.

Stable stratification restricts the vertical migration of fluid particles and hence the size of turbulent eddies so that throughout most of the boundary layer h is not an appropriate length scale and it is the local rather than surface fluxes which are relevant. The *local scaling hypothesis* (Nieuwstadt, 1984) constitutes a similarity approach to stable boundary layers. It postulates that (locally-scaled) dimensional combinations of variables can be expressed as functions of the single parameter z/Λ_{MO}, where Λ_{MO} is the *local* Monin-Obukhov length defined by

$$\Lambda_{MO} = \frac{|\underline{\tau}|^{3/2}}{\kappa(-G)} = \frac{|-\overline{u' w'}|^{3/2}}{\kappa \alpha g(-\overline{\theta' w'})} \tag{5.32}$$

In the limit as $z/\Lambda_{MO} \to \infty$ dimensionless combinations must approach constant values. This is the regime of *z-less stratification*. In particular, Richardson numbers Ri and R_f become constants.

Nieuwstadt (1984, 1985) derived an analytical model of the stable ABL in this constant-Richardson-number regime. His main assumptions were

(A1) Steady-state (in the sense of time-independent fluxes). As we have seen this leads to a heat flux varying linearly with height:

$$\overline{\theta' w'} = \overline{\theta' w'}_0 (1 - z/h) \tag{5.33}$$

(A2) Richardson numbers constant over the depth of the boundary layer; ie,

$$\begin{aligned} \frac{\alpha g \dfrac{d\Theta}{dz}}{\left|\dfrac{d\vec{U}}{dz}\right|^2} &= Ri, \quad constant \\ \frac{\alpha g(-\overline{\theta' w'})}{\vec{\tau}.\dfrac{d\vec{U}}{dz}} &= R_f, \quad constant \end{aligned} \tag{5.34}$$

(A3) Stress parallel to shear. Then, using complex variable notation with $\tau = \tau_{xz} + i\tau_{yz}$, $W = U + iV$, we have $\vec{\tau}.\dfrac{\partial \vec{U}}{\partial z} = \bar{\tau}\dfrac{\partial W}{\partial z}$ and hence, from (5.33) and (5.34),

$$\bar{\tau}\frac{\partial W}{\partial z} = \frac{B_0}{R_f}(1 - z/h) \tag{5.35}$$

where $B_0 = \alpha g(-\overline{\theta' w'})_0 = u_*^3/\kappa L_{MO}$ is the (downward) surface buoyancy flux.

We solve (5.35) in conjunction with the momentum equation

$$\frac{\partial \tau}{\partial z} = if(W - W_g) \tag{5.36}$$

Differentiating (5.36) with respect to z and substituting in (5.35) gives

$$\bar{\tau}\frac{\partial^2 \tau}{\partial z^2} = i\frac{B_0 f}{R_f}(1 - z/h) \tag{5.37}$$

This has the similarity solution

$$\tau = u_*^2 (1 - z/h)^{\alpha} \tag{5.38}$$

where equating exponents and multiplying factors yields

$$\begin{aligned} \alpha + \bar{\alpha} - 2 &= 1 \\ \alpha(\alpha - 1) &= i\frac{B_0 f h^2}{R_f u_*^4} \end{aligned} \tag{5.39}$$

from which it follows that

$$\alpha = \frac{3}{2} + i\frac{\sqrt{3}}{2}(\mathrm{sgn}\ f) \tag{5.40}$$

and

$$h^2 = \sqrt{3} R_f \frac{u_*^4}{B_0 |f|} = \sqrt{3}\kappa R_f \frac{u_* L_{MO}}{|f|} \tag{5.41}$$

This is readily identified with the Zilitinkevich (1989) formula for the stable boundary-layer height, $h=c(u_* L_{MO}/f)^{1/2}$, with a constant value $c \approx 0.4$.

The mean-velocity profile can now be obtained from the momentum equation:

$$\frac{W_g - W}{u_*} = \frac{1}{\kappa R_f}\frac{h}{L_{MO}} e^{-\frac{i\pi}{3}\mathrm{sgn}\ f} (1 - z/h)^{\left(\frac{1}{2} + i\frac{\sqrt{3}}{2}\mathrm{sgn}\ f\right)} \tag{5.42}$$

In particular, since $W=0$ on $z=0$, this implies a geostrophic velocity magnitude

$$\frac{|W_g|}{u_*} = \frac{1}{\kappa R_f}\frac{h}{L_{MO}} \tag{5.43}$$

and a wind direction shear of 60° over the depth of the boundary layer.

The mean potential temperature can be obtained from the assumption of constant gradient Richardson number:

$$\frac{\Theta - \Theta_0}{\theta_*} = -\frac{Ri}{\kappa R_f^2}\frac{h}{L_{MO}} \ln(1 - z/h) \tag{5.44}$$

Note the logarithmic singularity at the top of the boundary layer. Clearly, Nieuwstadt's model is inadequate here, but the profile does imply a large temperature inversion at this height.

Derbyshire (1990) has re-examined Nieuwstadt's model and lists the main criticisms levelled at the theory: the assumption of steady-state, singularity in the temperature profile at the top of the boundary layer, no explicit treatment of internal wave effects and the lack of consistency outside the strong stability limit. The ageostrophic wind angle (60°) is too large. Also, from (5.41) and (5.43) we deduce

$$B_0 = \frac{R_f}{\sqrt{3}} |W_g|^2 |f| \tag{5.45}$$

Thus, according to Nieuwstadt's theory, the downward surface heat flux is determined completely by the synoptic parameter $|W_g|$ whereas, in practice, it is an independent parameter. (In most cases the soil heat flux is comparatively small so that the sensible heat flux in the air balances the loss of heat by radiation, which is essentially determined by cloud cover.)

Despite these criticisms, Derbyshire (1990) goes on to identify the role of Nieuwstadt's model as the asymptotically valid case in the strong stability limit $h/L_{MO} \to \infty$. In this case (5.45) is identified as the maximum downward buoyancy flux.

In the moderately stable or neutral case and in the surface layer the least sustainable assumption of Nieuwstadt's model is that of constant R_f. Now, from the stress and velocity profiles and the corresponding flux and mean profiles for temperature we can deduce gradient transfer coefficients K_M and K_H for momentum and heat respectively:

$$\begin{aligned} K_M &= \kappa u_* R_f L_{MO} (1 - z/h)^2 \\ K_H &= \kappa u_* \frac{R_f^2}{Ri} L_{MO} (1 - z/h)^2 \end{aligned} \tag{5.46}$$

In an appendix to his 1985 paper Nieuwstadt proposes to match these to the surface-layer transfer coefficients; thus, for example,

$$K_M = \frac{\kappa u_* z (1 - z/h)^2}{1 + z/R_f L_{MO}} \tag{5.47}$$

which has the correct asymptotic behaviour in the limits $z/R_f L_{MO} \to \infty$ and $z/R_f L_{MO} \to 0$.

However the boundary-layer profiles cannot then be obtained in closed form and the equations must be solved numerically.

5.4 Other Atmospheric Boundary-Layer Closure Models

Holtslag and Nieuwstadt (1986) provide a useful regime diagram for the idealised stable/neutral/unstable ABL (Figure 5.1), illustrating the scaling parameters applicable in various regions of (z/h,h/L_{MO})-space. Diffusion models for these distinct regimes have been described by Gryning et al. (1987). In Sections 5.2 and 5.3 we reviewed analytical models of ABL structure in two particular regimes: the constant-flux, near-surface region described by Monin-Obukhov similarity theory and the constant-Richardson-number, local-scaling model of Nieuwstadt. Although highly successful in their own right (particularly surface-layer similarity theory which often applies over the entire depth covered by ground-based meteorological instruments), they represent the asymptotic behaviour in distinct regions of the flow and are not easily reconcilable. The same may be said of other attempts to match models across the boundaries in the regime diagram. To determine boundary-layer structure over the entire height and stability range one must resort to more complex turbulence equations, which may only be solved by numerical means.

Numerical modelling of ABL structure has been undertaken with all levels of turbulence closure in the hierarchy described in Chapter 4. An alternative hierarchy of turbulence models specifically for the atmospheric boundary layer has been developed over a number of years by Mellor and Yamada (1974, 1982), based on the systematic simplification of a second-order-closure model. Sub-models of various degrees of complexity were derived by neglecting terms of successive order in an anisotropy parameter a, where a is the magnitude (precise definition not specified) of the anisotropy tensor

$$a_{ij} = \frac{\overline{u_i' u_j'}}{k} - \frac{2}{3}\delta_{ij} \tag{5.48}$$

The fundamental (*level 4*) model is essentially a second-order-closure model, solving equations for the Reynolds stresses, scalar fluxes and scalar variances. The major difference

between this model and the Reynolds-stress transport models familiar to mechanical engineers is the use of a turbulence length scale l rather than turbulence dissipation rate ε as a scale-determining variable. In the original paper (Mellor and Yamada, 1974) the length scale was specified algebraically:

$$l = \frac{\kappa z}{1+\kappa z/l_{max}} \tag{5.49}$$

Later, this prescription was replaced by a prognostic equation for the turbulence length scale (strictly for kl). Mellor and Yamada maintain that the solution of an equation for turbulence dissipation is fundamentally unsound, but, equally, their model is *incomplete*, in the sense that geometry-dependent terms must appear in the scale-determining equation to return the correct behaviour near boundaries. The *level 3* model is essentially an algebraic stress model with transport equations for the turbulent kinetic energy but algebraic relations for the individual Reynolds stresses. The *level 2* model abandons advection and diffusion (ie, there are no turbulence transport equations), but retains algebraic forms for the production, dissipation and redistribution terms. *Level 1* corresponds roughly to a mixing-length model. In their 1982 consolidation work, Mellor and Yamada insert an intermediate *level 2½* model, abandoning the transport equation for the scalar fluctuations (by neglecting advection and diffusion) but retaining the full turbulent transport equation for k. It is, perhaps, unfortunate that the models developed by the engineering community are often distinct from those familiar to atmospheric physicists. The widely-used k-ε model, for example, has no place in Mellor and Yamada's system.

We return now to the application of more conventional engineering-type turbulence models to the idealised, spatially homogeneous ABL. One- and two-equation closures will be examined in more detail in Section 5.5. In the remainder of this Section a brief review of more complex models will be undertaken.

In a series of papers, Wyngaard et al. (1974), Wyngaard and Coté (1974) and Wyngaard (1975) used a second-order-closure model to examine the turbulence structure of steady-state neutral, evolving convective and evolving stable atmospheric boundary layers respectively. Interestingly, the stable boundary-layer simulations indicated approach to a steady state

(capped by an inversion) a few hours after transition. They also revealed the process of formation of a supergeostrophic nocturnal jet: essentially an inertial oscillation as turbulent transport collapsed at the top of the boundary layer.

Beyond the realms of single-point closures, both large-eddy simulation (LES) and direct numerical simulation (DNS) have been used to predict the structure of the atmospheric boundary layer. Both integrate the time-dependent Navier-Stokes equations. In LES the sub-grid scales have to be parameterised. In DNS the mesh is small enough for all relevant scales to be resolved. This means all scales from the Kolmogorov length $(\nu^3/\varepsilon)^{1/4}$ to the boundary-layer depth h, which imposes a severe restriction on accessible Reynolds numbers.

Large-eddy simulations have been performed for the neutrally stable ABL by Mason and Thomson (1987), for the convective ABL by Mason (1989) and for the stably stratified ABL by Mason and Derbyshire (1990). In the stable case a particularly important advantage of LES over conventional one-point closures is the ability to resolve explicitly both turbulence and waves. Mason and Derbyshire (1990) followed the time evolution of a stable ABL subject to constant heat flux or constant cooling rate at the lower boundary. Provided the downward heat flux was not sufficient to eradicate turbulence, both converged to qualitatively similar final states. This approach to a quasi-steady state is in line with the theoretical arguments of Derbyshire (1990) and the second-order-closure model of Wyngaard (1975). The simulations confirmed the usefulness of the local scaling concept (Nieuwstadt, 1984) and the apparently minor role played by wave radiation in energy transport over flat terrain.

Direct numerical simulation of the Ekman boundary layer is the subject of papers by Coleman et al. (1990) for the neutral ABL and Coleman et al. (1992) for the stably stratified ABL. In the latter case the simulations agreed well with Mason and Derbyshire's (1990) LES studies and once more confirmed the usefulness of the local-scaling concept. DNS profiles for the dissipation rate ε compared favourably with the models of Brost and Wyngaard (1978) (buoyancy length σ_w/N; velocity scale $k^{1/2}$) and Hunt et al. (1987) (shear length scale $\sigma_w/(dU/dz)$; velocity scale σ_w). More will be said about these models in the next Section.

5.5 A Limited-Length-Scale k-ε Model

In the vast majority of eddy-viscosity models (and many more complex models, too) it is commonly assumed that there is only one length scale and hence that the mixing length l_m and dissipation length $l_\varepsilon = u_0^3/\varepsilon$ are equal. That this need not be the case may be demonstrated by the following simple argument.

Consider a stably stratified equilibrium shear flow with mean velocity $U(z)$ and (kinematic) shear stress τ given by

$$\tau = \nu_t \frac{dU}{dz} \tag{5.50}$$

The eddy viscosity ν_t is the product of a mixing length l_m and velocity scale u_0. In this simple equilibrium layer

$$u_0 = l_m \frac{dU}{dz} \tag{5.51}$$

so that, on multiplying by u_0,

$$u_0^2 = \nu_t \frac{dU}{dz} = \tau \tag{5.52}$$

Hence $\tau^{1/2}$ is the appropriate velocity scale. But now, by local equilibrium:

$$P + G = \varepsilon \tag{5.53}$$

whilst, by the eddy-viscosity hypothesis for the shear stress,

$$P = \tau \frac{\partial U}{\partial z} = \frac{\tau^2}{\nu_t} \tag{5.54}$$

Hence, dividing (5.53) by (5.54) leads to

$$\nu_t = \frac{\tau^2}{\varepsilon}(1-\boldsymbol{R}_f) \tag{5.55}$$

where

$$\boldsymbol{R}_f \equiv -\frac{\boldsymbol{G}}{\boldsymbol{P}} \tag{5.56}$$

is the *flux Richardson number*, the ratio of the rate of removal of turbulent kinetic energy by buoyancy forces to its production by shear. Since the velocity scale is $\tau^{½}$, equation (5.55) represents a relation between length scales:

$$l_m = l_\varepsilon(1-\boldsymbol{R}_f) \tag{5.57}$$

Equation (5.55) is equivalent to the standard k-ε model in neutral flow if C_μ is the structure function $(\tau/k)^2$. Here, in the absence of better data, this is assumed to be the same as in neutral flow over the same surface, although Rodi (1987) suggests that τ/k is itself a function of R_f.

Note that the 1-R_f factor governs the ratio of mixing length to dissipation length. It is quite distinct from the rather more stringent Richardson-number dependency exhibited in the surface layer by the mixing length:

$$l_m = \kappa z(1-\beta \boldsymbol{R}_f) \ , \qquad \beta \approx 5 \tag{5.58}$$

We now come to the central premise of this Section: that, in many flows of interest, there is some *maximum* size of turbulent eddy - a scale defined, for example, by boundary-layer depth or imposed by stratification.

This is easily incorporated into one-equation models where the mixing length is specified algebraically; for example, in a simple shear flow:

$$\frac{1}{l_m} = \frac{1}{\kappa z} + \frac{1}{l_{max}} \tag{5.59}$$

or, equivalently,

$$l_m = \frac{\kappa z}{1 + \kappa z / l_{max}} \tag{5.60}$$

However, the k-ε model is essentially a single-length-scale model, with l_m identically equal to the dissipation length. In the above example the standard k-ε model will give a length scale growing approximately linearly with height.

Detering and Etling (1985), in their simulation of the Leipzig wind profile, concluded that the standard k-ε model when applied to the atmospheric boundary layer yields

- a very deep boundary layer
- large mixing length (and hence eddy viscosity) in the upper boundary layer
- large friction velocity
- small cross-isobar angle

when compared with observations. These deficiencies can all be traced to the inability of the k-ε model in its standard form to recognise some finite upper limit to the mixing length. By contrast a one-equation (k) model, with mixing length prescribed by (5.60), compared very favourably with experimental observations when an appropriate value of l_{max} was used.

There are thus two requirements of the new model: (i) to *specify* the maximum mixing length; (ii) to modify the two-equation turbulence model to accommodate l_{max}.

Dealing first with (i), l_{max} may be either a *global* (ie, fixed) scale, or one defined locally in terms of, for example, mean-flow gradients. We have found the former both more practical and more realistic. For example, in jet or wake flows l_{max} could be taken as proportional to the shear-layer thickness at each downwind station. In a neutral ABL simulation a typical maximum mixing length is

$$l_{max} = \frac{h}{3} \tag{5.61}$$

where the boundary-layer height h may be estimated from surface data as cu_*/f, $c \approx 0.2$ (Garratt, 1992).

In the stable ABL it is the Monin-Obukhov length L_{MO} which governs the size of the largest eddies, rather than the boundary-layer height h. As we have seen in Section 5.2, in the surface layer where vertical momentum and heat fluxes are essentially constant, Monin-Obukhov similarity theory gives for the eddy viscosity:

$$\nu_t = \frac{\kappa u_* z}{1 + \beta z/L_{MO}} \qquad \beta \approx 5 \tag{5.62}$$

The velocity scale is u_* and hence the mixing length is

$$l_m = \frac{\kappa z}{1 + \beta z/L_{MO}} \tag{5.63}$$

Comparison with (5.60) yields a maximum mixing length

$$l_{\max} = \frac{\kappa}{\beta} L_{MO} \approx 0.08\, L_{MO} \tag{5.64}$$

We come now to the second requirement of the new model: namely, to impose a maximum length scale through the turbulence equations. In the k-ε model the length-scale-determining equation is that for the dissipation rate ε. A change in the mixing length may be effected by adjusting the difference between production and removal terms in that equation.

Detering and Etling chose to limit the growth of the turbulent length scale in the upper part of the ABL by increasing the production term in the dissipation equation (increasing ε ⇔ decreasing l_m). In our notation, the production coefficient $C_{\varepsilon 1}$ would be replaced by

$$C_{\epsilon 1}\left(\frac{l_m}{\gamma h}\right) \tag{5.65}$$

With $h=0.2u_*/f$ the constant γ has the value 0.0075. (This model was also used to compute stably stratified flow over Steptoe Butte by Dawson et al., 1991). We too have chosen to limit the turbulent length scale by modifying the production term in the dissipation equation. However, in contrast to Detering and Etling, the modification is such that the model remains consistent with the logarithmic velocity profile for $z/h \ll 1$. As intimated earlier, the modification may be applied equally to other types of turbulent shear flow where there is some natural maximum mixing length.

Suppose then that there is some maximum mixing length l_{max} imposed, for example, by the depth of the boundary layer. The effect of the change should be dependent on the ratio l_m/l_{max} and operate to bring production and removal terms in the dissipation equation into balance when $l_m/l_{max} \approx 1$, whilst reducing to the standard form when $l_m/l_{max} \approx 0$. This is most simply achieved by reformulating the ε production term as

$$P_\epsilon = \left[C_{\epsilon 1} + (C_{\epsilon 2} - C_{\epsilon 1})\frac{l_m}{l_{max}}\right]\frac{\Pi}{\tau_\epsilon} \tag{5.66}$$

When $l_m \ll l_{max}$ (ie, close to the surface) the change is negligible and the equations remain consistent with the equilibrium-layer profiles. On the other hand, assuming local equilibrium ($\Pi=\varepsilon$), then source and sink terms cancel when $l_m=l_{max}$. The additional production term therefore acts as a feedback mechanism to oppose the turbulent length scale exceeding l_{max}. Note that, with the exception of l_{max}, the modification introduces no new constants into the model and may be applied with any *a priori* values of $C_{\varepsilon 1}$ and $C_{\varepsilon 2}$.

We shall now consider the application of the limited-length-scale k-ε model to the calculation of neutral and stably stratified ABL profiles. The application to perturbed atmospheric boundary layers will be demonstrated in the Cinder Cone Butte test case in Chapter 6.

5.5.1 Neutral Atmospheric Boundary-Layer Simulation

Detering and Etling (1985) used one- and two-equation turbulence models to predict the famous Leipzig wind profile (Lettau, 1950). Their standard *k*-ε computations were repeated (consistently!) with our own code SWIFT, and the resulting mean and turbulence profiles are shown in Figures 5.2-5.5. Experimental data in the graphs has been read from Detering and Etling's graphs.

To recap, for a horizontally homogeneous, steady-state, Coriolis boundary layer the horizontal momentum equations reduce to a balance between ageostrophic velocity and vertical stress divergence:

$$\begin{aligned} 0 &= f(V-V_g) + \frac{\partial \tau_{xz}}{\partial z} \\ 0 &= -f(U-U_g) + \frac{\partial \tau_{yz}}{\partial z} \end{aligned} \tag{5.67}$$

where the constant horizontal pressure gradients have been written in terms of the *geostrophic* wind velocity prevailing at the top of the boundary layer:

$$\begin{aligned} U_g &= -\frac{1}{\rho f}\frac{\partial P}{\partial y} \\ V_g &= \frac{1}{\rho f}\frac{\partial P}{\partial x} \end{aligned} \tag{5.68}$$

Shear stresses are described by eddy-viscosity models

$$\tau_{xz} = \nu_t \frac{\partial U}{\partial z}, \qquad \tau_{yz} = \nu_t \frac{\partial V}{\partial z} \tag{5.69}$$

with ν_t given by *k* or *k*-ε models as described earlier.

The boundary-layer parameters used were as follows.

geostrophic wind speed: U_g=17.5 m s^{-1}

Coriolis parameter: f=1.13x10^{-4}s^{-1}

roughness length: z_0=0.3m

The experimental measurements indicated a surface wind turned by 26.1° from the geostrophic and a friction velocity u_*=0.65 m s^{-1}.

Simulations of the Leipzig experiment have been carried out with the SWIFT code using limited- and unlimited-length-scale k and k-ε models of turbulence. Figures 5.2-5.5 show computed profiles of mean wind speed and direction, turbulent kinetic energy and mixing length. The maximum mixing length l_{max} was applied either directly through the length-scale formulation (equation (5.60)) for the one-equation model or through the dissipation production term (equation (5.66)) for the k-ε model. In the limited-length-scale cases an externally specified value l_{max}=36m was chosen, based on the analysis of the Leipzig data by Blackadar (1962).

The effect of length-scale-limiting is quite gratifying. A shallow boundary layer is now evident, the cross-isobar surface wind direction (26°) is close to the measured value, and the turbulent kinetic energy falls off significantly over the depth of the boundary layer. This is in contrast to the unlimited form of the models where, due to excessive turbulent diffusion, the wind speed has not settled on the geostrophic at the upper limit of the computational domain (z_{max}=3000m), no low-level jet is apparent and the wind-direction shear over the height of the boundary layer is about half the measured value.

What is most significant, however, is that results of length-scale-limited k-ε and one-equation models are almost coincident for the same value of l_{max}. What we have shown, therefore, is that, for turbulence near equilibrium at least, the modification (5.66) to the dissipation equation *is* a suitable means of limiting the turbulent length scale. This is confirmed by the mixing-length plot in Figure 5.5 where the predicted mixing length is maintained close to the externally specified maximum value of 36m, rather than growing nearly linearly with height as in the standard model.

Over flat terrain the k-ε model has no advantages over the simpler one-equation model, since

the *a priori* length scale is necessarily proportional to the distance from the surface. Its advantage lies in computing geometrically complex flows since in those cases the dissipation length scale is not available from similarity. The same *maximum* mixing length will, however, still apply.

For neutrally stratified shear flows along plane walls turbulent eddies are restricted in size by the boundary-layer depth. A typical maximum mixing length is $h/3$. This is rather difficult to reconcile with the Leipzig data, for which $l_{max}\approx 36$m, whereas the boundary layer depth was of order several hundred metres. However, it is now generally recognised that the Leipzig experiment was actually conducted in slightly stable conditions. In these circumstances the relevant length is the Monin-Obukhov length L_{MO} for which, as we have seen, surface-layer similarity argues for $l_{max}\approx 0.08 L_{MO}$. This would be much more realistic in this case. The stably stratified ABL will be considered in the next Section.

5.5.2 Stable Atmospheric Boundary-Layer Simulation

The limited- and unlimited-length-scale k-ε models were used to compute vertical profiles for a boundary layer with the following parameters:

geostrophic wind speed:	U_g=7.06m s^{-1}
Coriolis parameter:	f=1.13×10^{-4}s^{-1}
roughness length:	z_0=0.3m
boundary-layer height:	h=200m
Monin-Obukhov length:	L_{MO}=100m
surface heat flux:	Q_H=-20W m^{-2}

Values were chosen to be consistent with standard formulae for stable boundary-layer depth (Van Ulden and Holtslag (1985):

$$h = 0.4\left(\frac{u_* L_{MO}}{f}\right)^{1/2} \tag{5.70}$$

and drag parameter (Nieuwstadt, 1984):

$$\frac{U_g}{u_*} = \frac{1}{\kappa R_f}\frac{h}{L_{MO}} \tag{5.71}$$

The heat flux and Monin-Obukhov length imply a friction velocity u_*=0.28 m s^{-1}. These formulae are clearly only meaningful in terms of a quasi-steady stable boundary layer and so the policy suggested in Section 5.1.2 was adopted whereby the temperature difference between a given height and the surface was computed, the global cooling of the boundary layer then entering as a source term in the temperature equation for $z<h$. In the absence of localised sources of heat (for example, latent heat release or radiative flux divergence) the thermal boundary-layer height is fixed, with heat fluxes varying linearly between z=0 and $z=h$. The actual temperature rise across the boundary layer is determined by the eddy-viscosity profile and must be computed. Consistent temperature boundary conditions are Θ=0 on z=0 and $\partial\theta/\partial z$=0 on $z=z_{max}$.

Figure 5.6-5.10 illustrate the difference between k-ε calculations of mean-velocity and turbulence profiles with and without length-scale limiting. The maximum mixing length calculated for this value of the Monin-Obukhov length is l_{max}=8m and Figure 5.9 demonstrates the efficiency with which the scheme restricts the mixing length (strictly, the dissipation length) to this value. Figures 5.6 and 5.7 show the wind speed profile and angle from geostrophic. For the limited-length-scale calculation a super-geostrophic jet is apparent at low levels and, in contrast with the unlimited case, wind speed and direction assume their geostrophic values at around 500m. Turbulence levels are lower and fall off more steeply with height (Figure 5.8). The consequence is a much greater turning of the wind with height (32° as opposed to 15°). The near-surface turbulent kinetic energy computed from the theoretical value of u_* is $C_\mu^{-1/2}u_*^2$=0.14 m^2 s^{-2} which is much more consistent with the length-limited version than the standard k-ε model. This is despite the fact that the additional term in the dissipation equation vanishes near the surface.

Finally, we consider the predicted temperature profiles (Figure 5.10). Note that the *temperature* flux is explicitly determined by our quasi-steady assumption (it falls off linearly over the depth of the boundary layer and vanishes above) and, therefore, the overall temperature rise depends on the (reciprocal of) the eddy viscosity:

$$\frac{d\Theta}{dz} = \frac{-\overline{\theta' w'}}{\nu_t/\sigma_\theta} = \frac{-\overline{\theta' w'}_0(1-z/h)}{\nu_t/\sigma_\theta}, \qquad (z<h) \tag{5.72}$$

In reality, a (time-dependent) temperature inversion would be expected to develop at the top of the boundary layer.

Local Restrictions on Vertical Mixing

The computations described hitherto have used a constant l_{max} to determine the limit on vertical mixing imposed by stratification. It could be argued that in very stably stratified flow the direct effects of the surface become negligible for $z \gg L_{MO}$ and, in this case, the appropriate length scale is proportional to the *local Monin-Obukhov length* Λ_{MO}, where

$$\Lambda_{MO} = \frac{\tau^{3/2}}{\kappa(-G)} \tag{5.73}$$

This is the basis of the *local scaling hypothesis* of Nieuwstadt (1984). As an interesting aside, we find that, taking $l_{max}=(\kappa/\beta)\Lambda_{MO}$ and assuming $\tau/k=C_\mu^{1/2}$, the ratio of length scales becomes

$$\frac{l_\epsilon}{l_{max}} = \beta\frac{(-G)}{\epsilon} \tag{5.74}$$

With the further assumption of local equilibrium ($P+G=\epsilon$) the production term in the dissipation equation becomes

$$P_\epsilon = C_{\epsilon 1}(1+C'_{\epsilon 3}R'_f)\frac{\Pi}{\tau_\epsilon} \tag{5.75}$$

where

$$R'_f = -\frac{G}{P+G}, \qquad C'_{\epsilon 3} = \beta\frac{C_{\epsilon 2}-C_{\epsilon 1}}{C_{\epsilon 1}} \tag{5.76}$$

This is of precisely the same form as Rodi's modification (Rodi, 1987) although in this case the constant $C'_{\epsilon 3}$ is somewhat larger, 1.67 as opposed to 0.8.

Another candidate for a limit on vertical mixing is the *buoyancy length scale* $c_B\sigma_w/N$ (Brost and Wyngaard, 1978; Pearson et al., 1983). This assumes equipartition of energy between the vertical component of turbulent kinetic energy $\frac{1}{2}\rho\sigma_w^2$ and potential energy $\frac{1}{2}\rho N^2 Z^2$ of a particle performing simple harmonic motion with rms amplitude Z. As with the standard argument leading to the concept of a dividing streamline in flow around topography this neglects both viscosity and, more seriously, the influence of pressure forces, which, in this instance, serves to redistribute energy amongst components and invalidate the formula near the surface. The constant c_B can be deduced by equating the buoyancy length $c_B\sigma_w/N$ to the maximum mixing length already deduced for the surface layer, $\frac{\kappa}{\beta}L_{MO}$, and substituting for N from the large height ($z/L_{MO}\rightarrow\infty$) limit of N from Monin-Obukhov similarity theory (equation (5.30)). The result is

$$c_B = \frac{1}{a_w\sqrt{\beta}} \approx 0.34 \tag{5.77}$$

where $a_w=\sigma_w/u_*\approx 1.3$. However, computations indicated better performance with the original Brost and Wyngaard value $c_B=0.68$.

Measurements at the Boulder Atmospheric Observatory (Hunt et al., 1985) were interpreted as showing that in many circumstances it is the *shear length scale* $\sigma_w/|\partial\vec{U}/\partial z|$ rather than the buoyancy length scale σ_w/N which determines the scale of vertical velocity fluctuations and hence of vertical momentum transport. In this case the effect of buoyancy forces on the length scale is indirect: reduced turbulence levels admitting greater velocity shear $|\partial\vec{U}/\partial z|$. In their *shear-blocking-mixing-length model* Hunt et al. (1987) suggested

$$\frac{1}{l_m} = \frac{A_B}{\kappa z} + \frac{A_S|\partial\vec{U}/\partial z|}{\sigma_w} \tag{5.78}$$

where, to be consistent with neutral surface layer profiles, "blocking" and "shear" constants A_B and A_S respectively must satisfy

$$A_B + \frac{A_S}{a_w} = 1 \tag{5.79}$$

The recommended values are $A_B=0.6$ and $A_S=1.0$. Since a proportion of the "distance-from-

the-wall" mixing length (κz) has been reassigned to the shear component it is difficult to put this model in the maximum-mixing-length form (5.59). For the purposes of comparison in the context of a limited length scale k-ε model we have assumed a maximum mixing length $\sigma_w/|\partial\vec{U}/\partial z|$.

Both buoyancy (σ_w/N) and shear ($\sigma_w/|\partial\vec{U}/\partial z|$) length scales have been tested indirectly by large-eddy simulation (Mason and Derbyshire, 1990) and direct numerical simulation (Coleman et al., 1992). However, the jury is still out as to which is the preferred option.

For completeness we list the four candidates we have chosen for l_{max} in the context of a limited-length-scale k-ε model.

$c_L L_{MO}$	Monin-Obukhov length; (c_L=0.08)
$c_L \Lambda_{MO}$	local Monin-Obukhov length
$c_B \sigma_w/N$	buoyancy length; (c_B=0.68)
$c_S \sigma_w/\lvert\partial U/\partial z\rvert$	shear length; (c_S=1.0)

Of these, only the first is a *fixed* length scale; the others all depend on *local* gradients. Within the framework of a two-equation eddy-viscosity model we are obliged to accept proportionality of the different stress components so that $\sigma_w = a_w\tau^{1/2} = a_w(C_\mu^{1/4}k^{1/2})$.

When these candidates for l_{max} are applied with the stable boundary-layer parameters described in the previous Section the predicted wind-speed profiles are shown in Figure 5.11. Only the fixed l_{max} depending on the surface Monin-Obukhov length provides a satisfactory boundary-layer profile. When the buoyancy length scale is used there is too much mixing at upper levels (with the prescribed heat flux profile the buoyancy frequency vanishes above $z=h$). Both local Monin-Obukhov length and shear mixing length are too small near the surface. The shear length scale model was also computationally difficult because of positive feedback:

increasing $\partial U/\partial z$ $\longrightarrow$ decreasing l_{max} $\longrightarrow$ decreasing ν_t $\longrightarrow$ increasing $\partial U/\partial z$

We conclude that, in the context of a limited-length-scale k-ε model at least, a single maximum mixing length based on the surface Monin-Obukhov length is both computationally straightforward and produces the most satisfactory shallow stable boundary layer.

5.5.3 Comparison With Cardington Data

In the previous Section we demonstrated the need for some modification to the length-scale-determining equation (in this case, dissipation) in order to generate a realistic stable boundary layer. Now, this boundary layer is clearly an idealised case since, in practice, measurements of the stable ABL are plagued by sensitivity to "non-ideal" influences such as terrain undulations, gravity waves and intermittent turbulence. Experimental data free of these influences is comparatively sparse, even for apparently flat measurement sites.

In this Section the limited-length-scale k-ε model was used to simulate measurements of wind and temperature profile measurements undertaken by the United Kingdom Meteorological Office at Cardington airfield (S.H. Derbyshire, private communication). Detailed wind and temperature profiles were taken using a tethered balloon. The particular experimental data used here was taken from run E4 on 8th March, 1993 between times 21:24 and 21:58 GMT, when a surface inversion of depth a few hundred metres was observed to have formed.

Parameters required for the particular test case are:

geostrophic wind speed, U_g

thermal boundary-layer depth, h

Monin-Obukhov length, L_{MO}

Additional dimensional quantities are the Coriolis parameter f (taken as $1.13\times10^{-4}\text{s}^{-1}$) and the surface roughness length z_0 (estimated as 0.1m).

Since upper-level winds were unavailable the geostrophic wind speed and direction had to be set equal to the values at the highest measuring point (425m): 14.1m s^{-1} and 135.3° respectively. Turbulent fluxes are notoriously difficult to measure, particularly in the atmosphere. In this instance a linear fit to the heat flux data was used to obtain a surface temperature flux $\overline{\theta' w'}_0$=-1.07×10^{-2}K m s^{-1} and thermal boundary-layer depth h=337m. An average of the shear stress measurements from below 100m gave a friction velocity u_*=0.208 m s^{-1}. The surface heat and momentum fluxes then implied a Monin-Obukhov length L_{MO}=60m.

Figures 5.12 and 5.13 compare predictions of the mean wind speed and direction with the experimental data. Speed predictions are generally on the high side although the maximum wind speed is well-predicted. Reliance on the highest measurement point to provide the geostrophic wind speed is deemed unsatisfactory. However, the agreement in wind direction shear is apparently quite good as is, in fact, the temperature rise over the depth of the boundary layer (2°C).

Figure 5.14 shows predictions of the flux Richardson number R_f. Perhaps surprisingly the maximum value occurs towards the top of the boundary layer rather than the middle, but this has, in fact, also been demonstrated in LES simulations (Derbyshire, 1990).

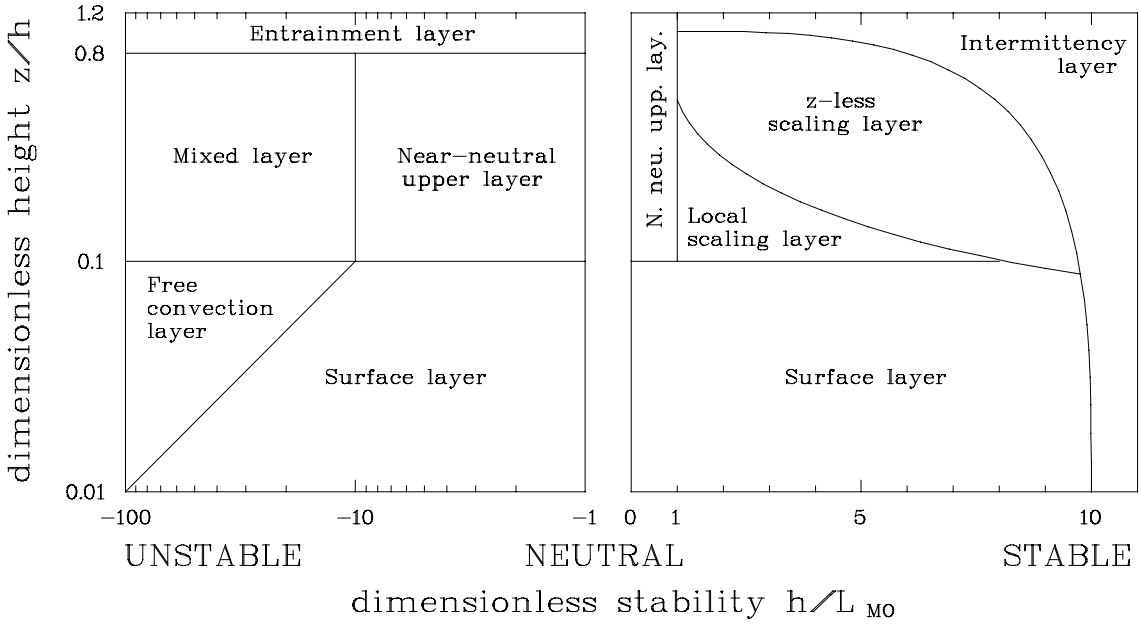

Figure 5.1: Regime diagram for the horizontally homogeneous atmospheric boundary layer (from Gryning et al., 1987).

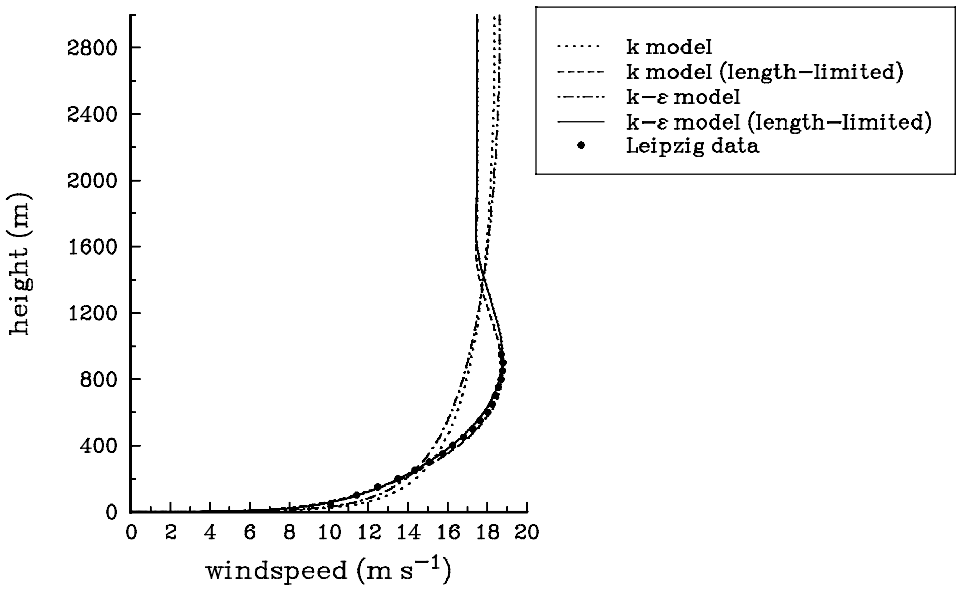

Figure 5.2: Simulation of Leipzig data: mean wind speed profile.

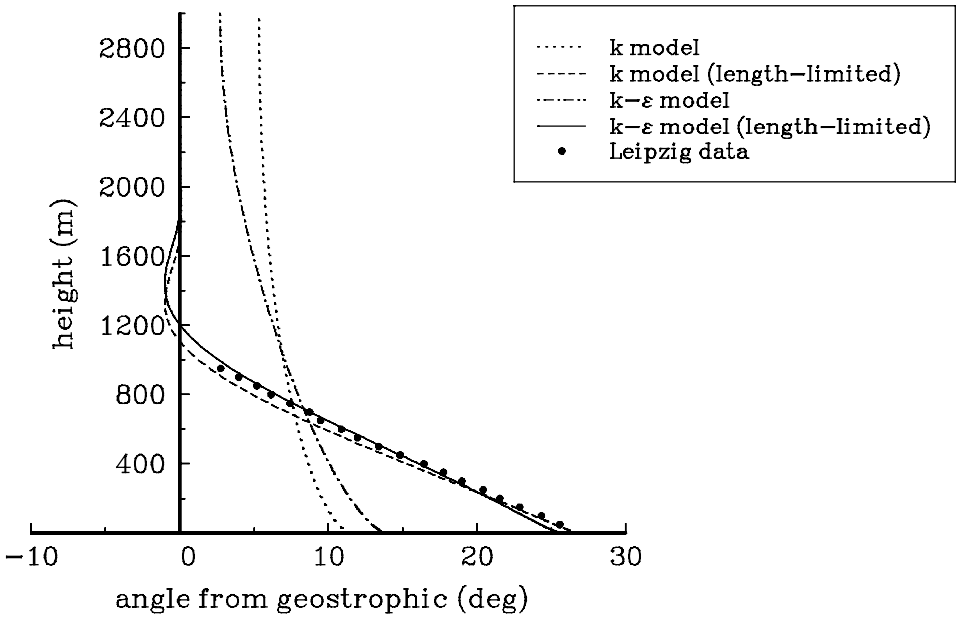

Figure 5.3: Simulation of Leipzig data: turning of wind with height.

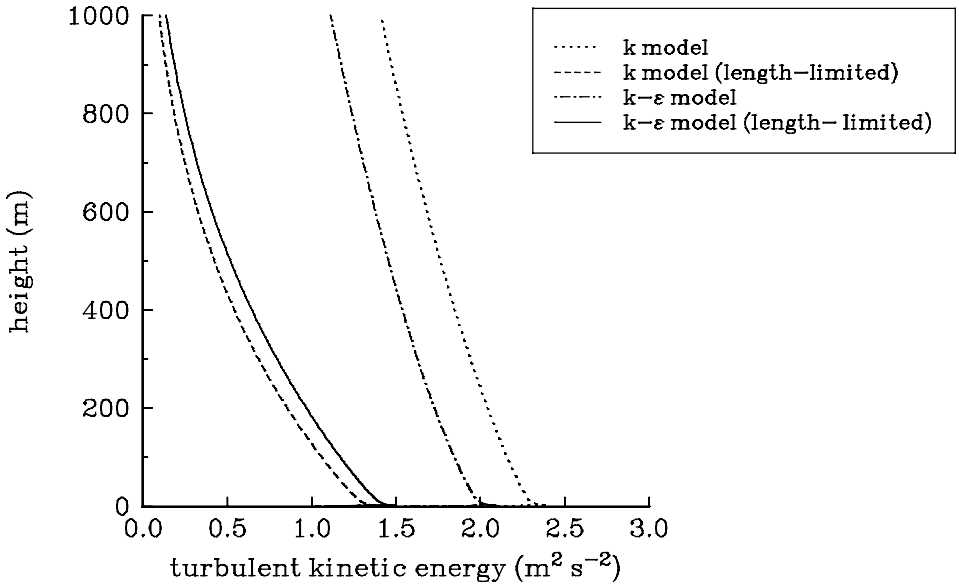

Figure 5.4: Simulation of Leipzig data: turbulent kinetic energy profile.

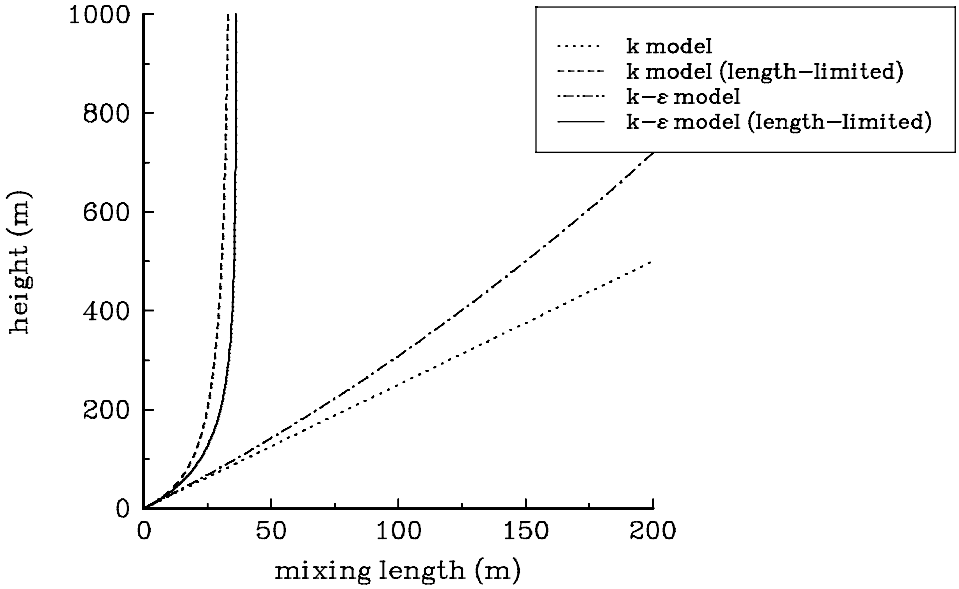

Figure 5.5: Simulation of Leipzig data: mixing-length profile.

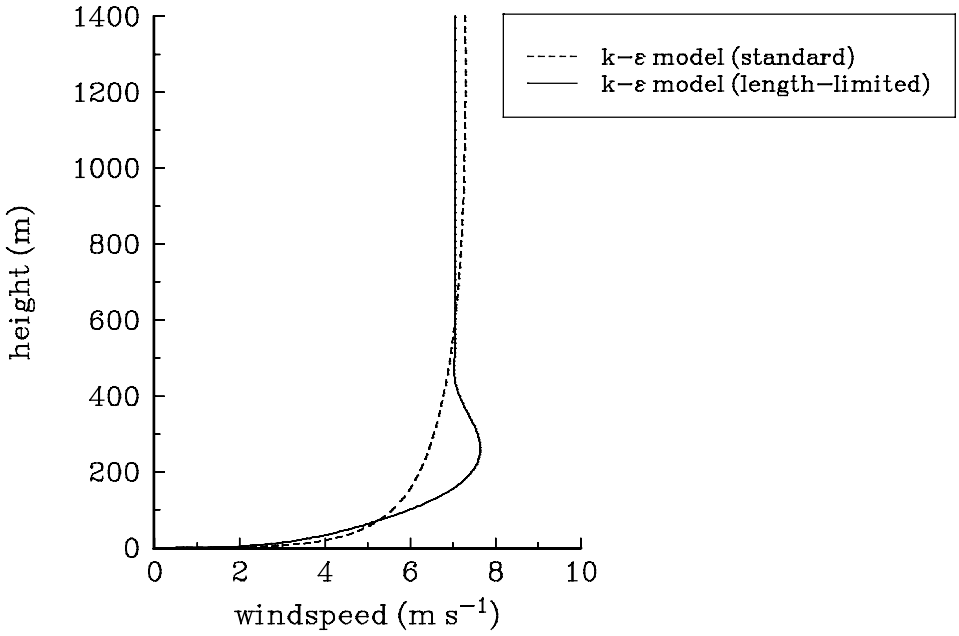

Figure 5.6: Stable boundary-layer simulation: mean wind speed profile.

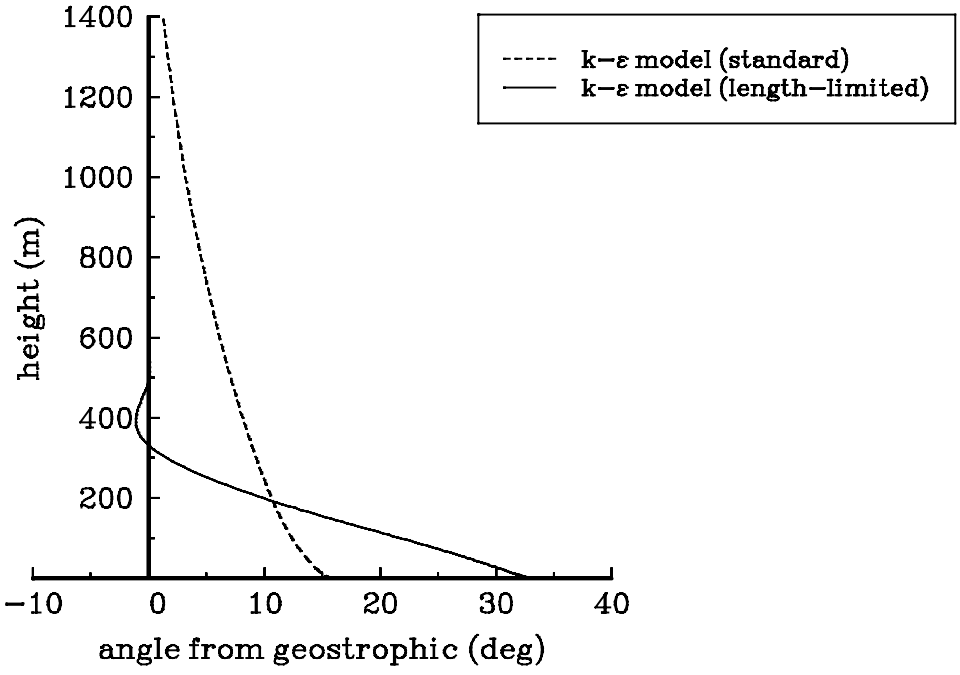

Figure 5.7: Stable boundary-layer simulation: turning of wind with height.

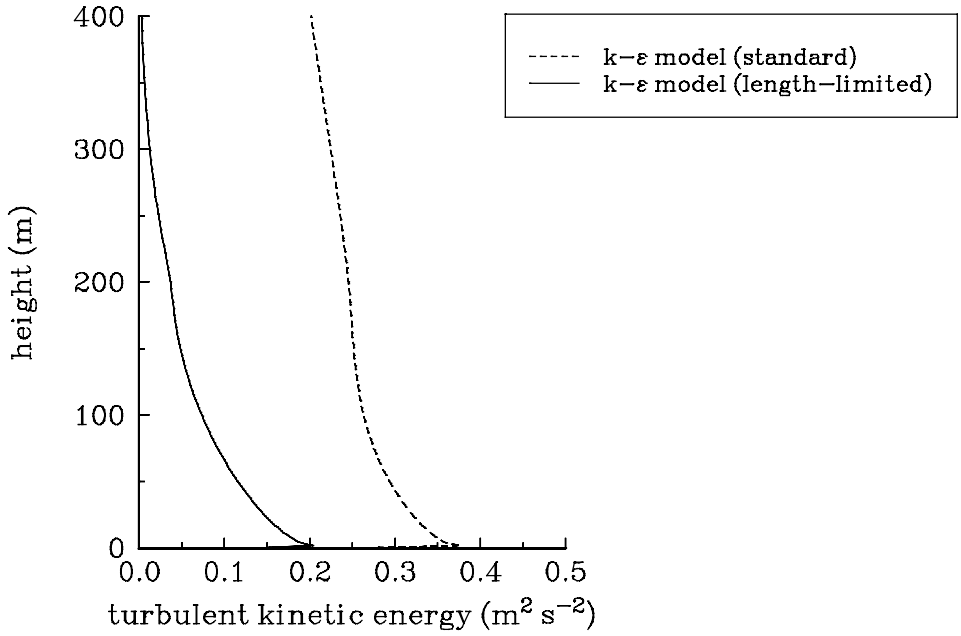

Figure 5.8: Stable boundary-layer simulation: turbulent kinetic energy profile.

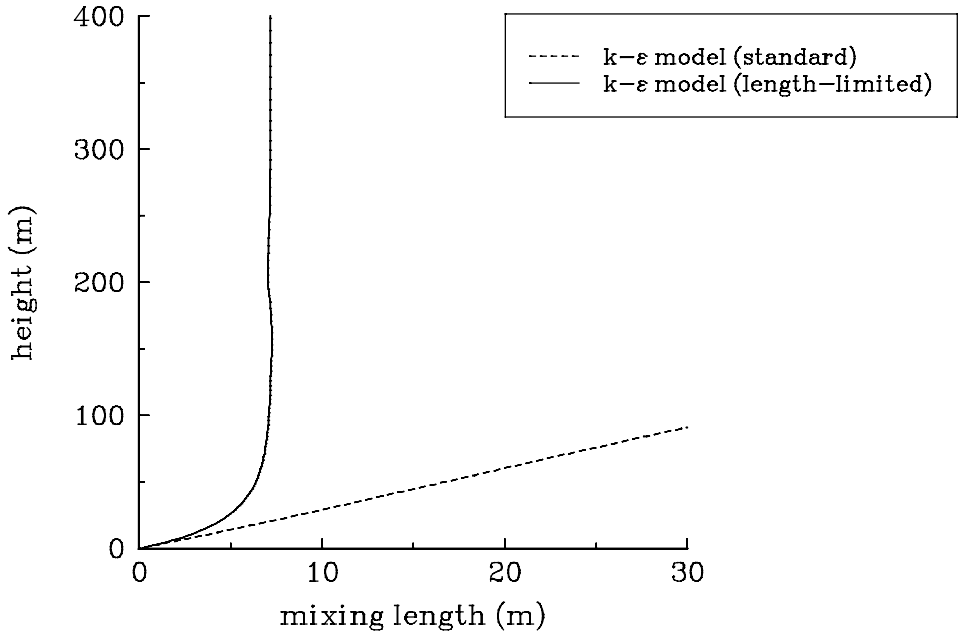

Figure 5.9: Stable boundary-layer simulation: mixing-length profile.

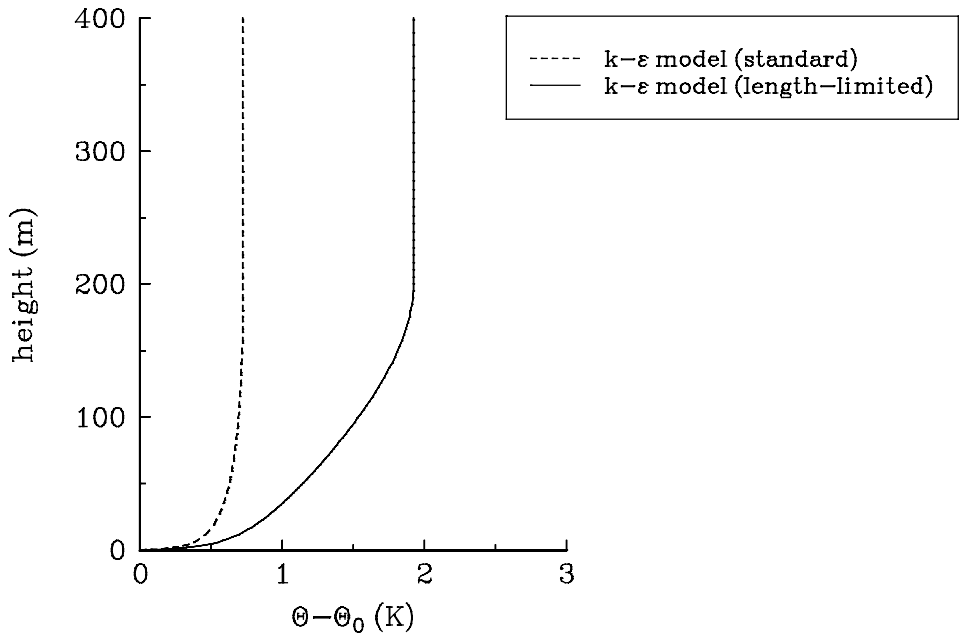

Figure 5.10: Stable boundary-layer simulation: mean temperature profile.

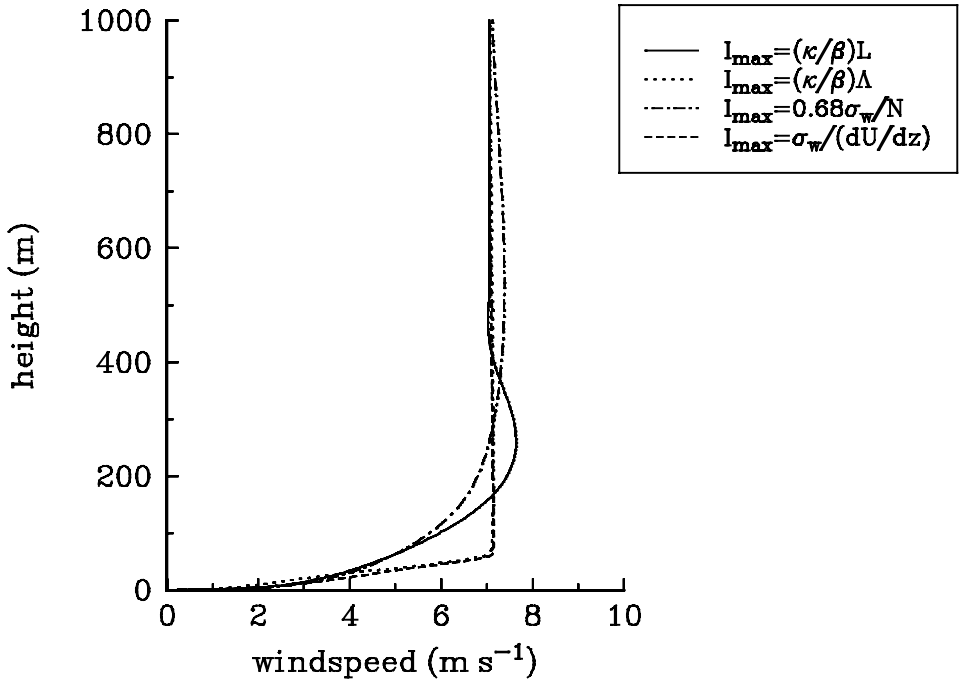

Figure 5.11: Stable boundary-layer simulation: different limits on vertical mixing.

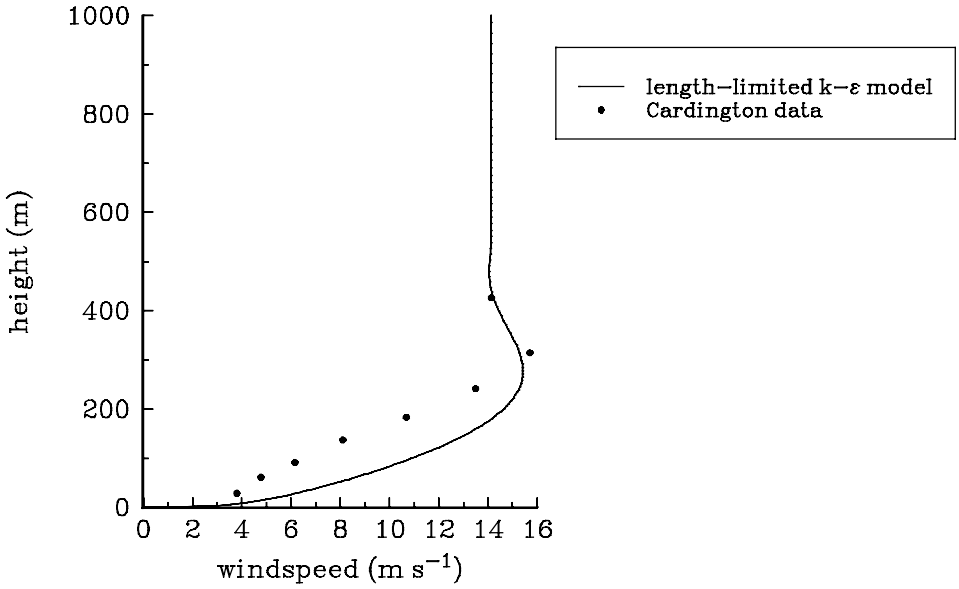

Figure 5.12: Simulation of Cardington data: mean wind speed profile.

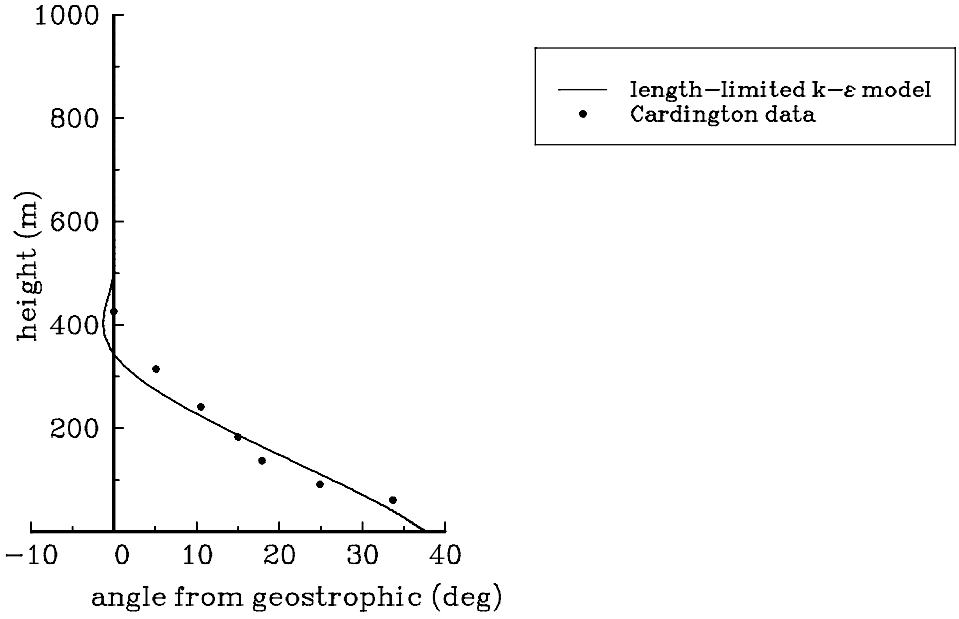

Figure 5.13: Simulation of Cardington data: turning of wind with height.

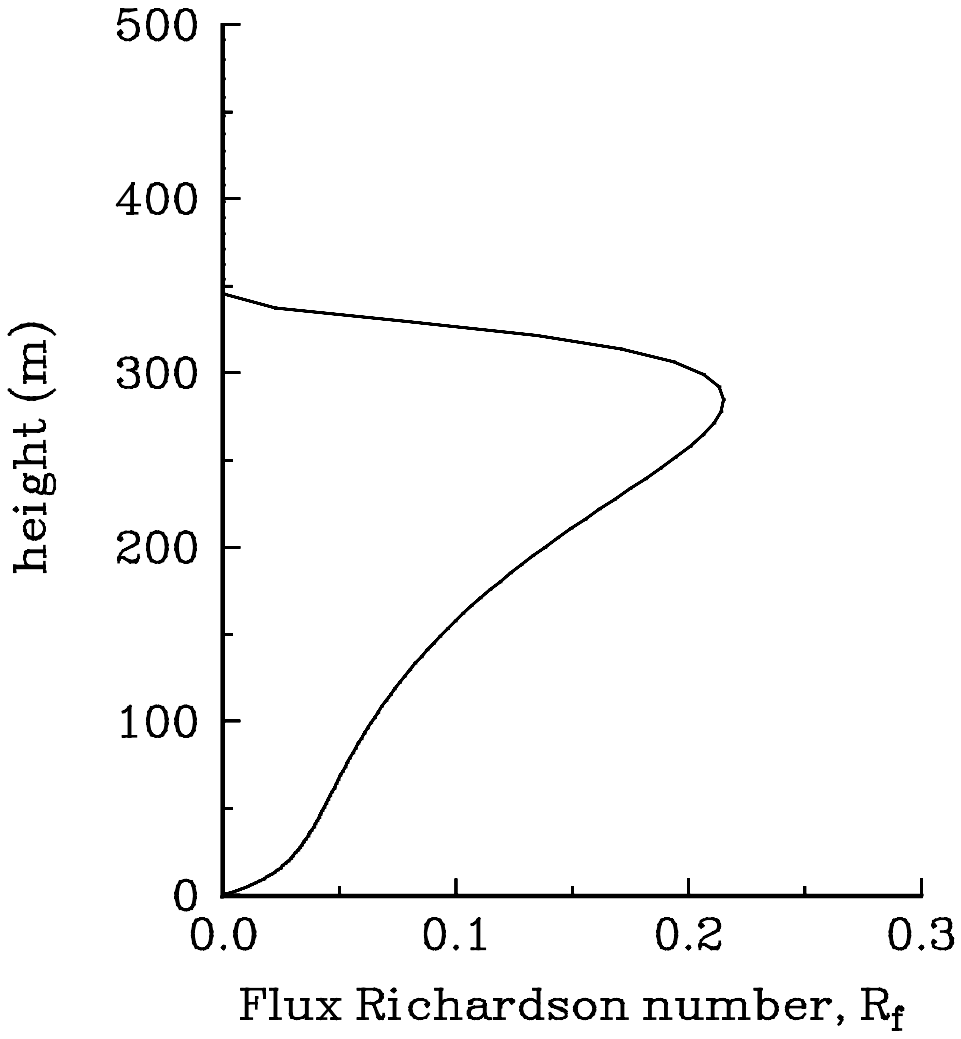

Figure 5.14: Simulation of Cardington data: flux Richardson number profile.